Journal Name

ARTICLE

Effect of particle concentration on the microstructural and macromechanical properties of biocompatible magnetic hydrogels

Received 00th January 20xx,
Accepted 00th January 20xx

DOI: 10.1039/x0xx00000x

www.rsc.org/

A. B. Bonhome-Espinosa,[1,2] F. Campos,[2,3] I. A. Rodriguez,[3] V. Carriel,[2,3] J. A. Marins,[4] A. Zubarev,[5] J. D. G. Duran[1,2] and M. T. Lopez-Lopez[1,2*]

We analyze the effect of nanoparticle concentration on the physical properties of magnetic hydrogels consisting of polymer networks of human fibrin biopolymer with embedded magnetic particles, swollen by a water-based solution. We prepared these magnetic hydrogels by polymerization of mixtures consisting mainly of human plasma and magnetic nanoparticles with OH^- functionalization. Microscopic observations revealed that magnetic hydrogels presented some cluster-like knots that were connected by several fibrin threads. By contrast, nonmagnetic hydrogels presented a homogeneous net-like structure with only individual connections between pairs of fibers. The rheological analysis demonstrated that the rigidity modulus, as well as the viscoelastic moduli, increased quadratically with nanoparticle content following a square-like function. Furthermore, we found that time for gel point was shorter in the presence of magnetic nanoparticles. Thus, we can conclude that nanoparticles favor the cross-linking process, serving as nucleation sites for the attachment of the fibrin polymer. Attraction between the positive groups of the fibrinogen, from which the fibrin is polymerized, and the negative OH^- groups of the magnetic particle surface qualitatively justifies the positive role of the nanoparticles on the enhancement of the mechanical properties of the magnetic hydrogels. Indeed, we developed a theoretical model that semiquantitatively explains the experimental results by assuming the indirect attraction of the fibrinogen through the attached nanoparticles. Due to this attraction the monomers condense into nuclei of dense phase and by the end of the polymerization process the nuclei (knots) of the dense phase cross-link the fibrin threads, which enhances the mechanical properties.

1 Introduction

Hydrogels are systems consisting of flexible polymer chains cross-linked within a continuous aqueous medium. Due to the versatility of the properties (mechanical, chemical, biocompatibility degree) of hydrogels, depending on their composition and preparation protocols, different applications have been reported for these materials in several fields, including biomedical engineering.[1,2] For example, in the field of tissue engineering, several hydrogels have been used as scaffolds that mimic the extracellular matrix of native tissues, such as cornea, oral mucosa, cartilage, peripheral nerve or bladder[3-7]. Another example is the use of porous hydrogels or hydrogels with microchannels for the delivery of drugs and cells.[8-10]

The fundamental investigation of the rheological properties of gels is an active field of research,[11-13] that presents special challenges due to possible changes in structure,[14] solvent loss[15] and wall slip effects.[11,15] Many rheological studies have focused on the steady-state storage modulus, gelation kinetics and sol-gel transition of hydrogels.[13,16-19] Of particular interest is the study of the gel point that can be defined as the point at which crosslinking polymers undergo phase transition from liquid to solid.[20] Consequently, at the gel point the steady shear viscosity tends to infinite. Several rheological methods have been used to detect the gel point. For example, many studies have extensively used the crossover point of the storage modulus (G') and the loss modulus (G''), although this method would only be correct if $G'(\omega)=G''(\omega)$ for any frequency of oscillation ω.[21] A more general method to detect the gel point is the Winter Chambon criterion that identifies this with the point at which $\tan\delta=G''/G'$ is frequency independent.[22] There are several approaches for practical application of Winter Chambon criterion. First, measurements may simply involve frequency sweeps, although this is a tedious and time-consuming approach that in addition is exposed to sample variability. A more sophisticated approach is Fourier Transform Mechanical Spectroscopy (FTMS), in which the sample is simultaneously subjected to several harmonic frequencies in a

[1] Department of Applied Physics, University of Granada, Granada, Spain.
[2] Instituto de Investigación Biosanitaria ibs.GRANADA, Granada, Spain.
[3] Department of Histology (Tissue Engineering Group), University of Granada, Granada, Spain.
[4] Laboratory of Condensed Matter Physics, University of Nice-Sophia Antipolis, CNRS, UMR No. 7336, Nice, France.
[5] Department of Mathematical Physics, Ural Federal University, Ekaterinburg, Russia.
* Corresponding author. Email: modesto@ugr.es

composite waveform, and the response is subsequently analyzed by Fourier transform.[17,23,24] An alternative to FTMS is Optimal Fourier Rheometry, in which the sample is subjected to a multi-frequency signal involving frequency modulated waveforms.[18,25]

In addition to polymer and water, hydrogels may contain other materials that modify their properties, such as synthetic nano- or microparticles. We refer to these materials as nanocomposites hydrogels, or even as bionanocomposites hydrogels if all their constituents are biocompatible materials. An example of nanocomposites hydrogels are the so-called magnetic hydrogels, which are characterized by the magnetic particles that are embedded within the polymer matrix.[26] The presence of magnetic material within this kind of hydrogels allows their detection and control by noncontact methods.[27-30] This is a clear advantage of magnetic hydrogels with respect to nonmagnetic ones and it is one of the reasons for the increasing attention that magnetic hydrogels are drawing. As a consequence, a number of studies on this field of magnetic hydrogels have been reported in the last few years.[26-46]

Several advantages have been reported in these previous works for magnetic hydrogels in the field of biomedicine, including the following. First, the presence of magnetic particles allows visualization and in-vivo follow-up by magnetic resonance imaging.[45] Furthermore, there is experimental in vitro evidence that suggests that the presence of magnetic materials within the hydrogels stimulates cell adhesion and proliferation.[31,32,47] Even more, it was recently demonstrated that when the presence of magnetic materials within the scaffolds was combined with application of a static magnetic field, a synergic effect in the osteoblastic differentiation of primary mouse calvarium osteoblasts was obtained.[48] In addition, the use of magnetic hydrogels in *in vivo* applications would allow attracting them to functionalized magnetic nanoparticles (MNP) injected close to them by the action of an applied magnetic field.[32,39,45] In tissue engineering applications this represents an interesting strategy to guide and concentrate growth factors, drugs and cells attached to the injected magnetic particles. Finally, very recently the preparation of artificial tissue-like hydrogels with magnetic field-depending mechanical properties has been reported.[27,29,30] This characteristic would allow the adjustment by noncontact magnetic forces of the mechanical properties of artificial magnetic hydrogels to native tissues at the site of implantation in tissue engineering applications, which represents a unique advantage with respect to nonmagnetic hydrogels.

Interestingly, a substantial enhancement of the mechanical properties of magnetic hydrogels with respect to nonmagnetic ones was also reported in the absence of applied magnetic fields in these previous works.[27,29,30] For example, a twofold to threefold increase of the storage modulus was found for fibrin-agarose hydrogels containing around 1 vol.% of magnetic particles with respect to the storage modulus of hydrogels without magnetic particles.[27,29,30] Note that this increase was not connected to the magnetic character of the particles, as demonstrated by using nonmagnetic particles, for which a similar enhancement was obtained.[27] Such an increase was much higher than the one predicted by the classical theory of mechanics of composite materials for a continuous matrix with spherical, completely rigid inclusions[49] and, thus, its origin must be in changes in the internal structure of the hydrogels when nanoparticles were included in the formulation. In this context, the aim of the present study is to characterize such an enhancement of the mechanical properties and to investigate its microscopic origin. In order to focus on the interaction between the nanoparticles and the fibrin polymer we investigated for this work fibrin hydrogels as simple as possible, without addition of agarose (a polysaccharide), which was used in previous works to give consistence to the resulting fibrin-agarose hydrogels. We prepared hydrogels at different concentrations of MNP and analyzed their macroscopic appearance, microscopic structure, swelling behavior, rheological properties and gelling time. As it will be shown below, we found dramatic changes in the macroscopic properties of the hydrogels when particle concentration was increased, which correlated well with changes in the microscopic structure.

2 Materials and Methods

2.1 Materials

For the preparation of the hydrogels, we used frozen human plasma obtained from blood donors (provided by the Granada Biobank of the Andalusian Regional Government). Aliquots of plasma were thawed by placing them at 37 ºC for 10 min immediately before use. As magnetic phase for the preparation of the magnetic hydrogels, we used MagP-OH nanoparticles supplied by nanoMyP® (Spain) as previously described.[27] These particles consisted of a multicrystalline magnetite (iron oxide) core (90 % v/v) and a polymeric layer (10% v/v) functionalized with OH^- groups –see (Fig. 1). The mean hydrodynamic diameter of MagP-OH particles was 110 nm, as measured by dynamic light scattering with a Zetasizer instrument (Malvern instruments, USA). The polymeric layer

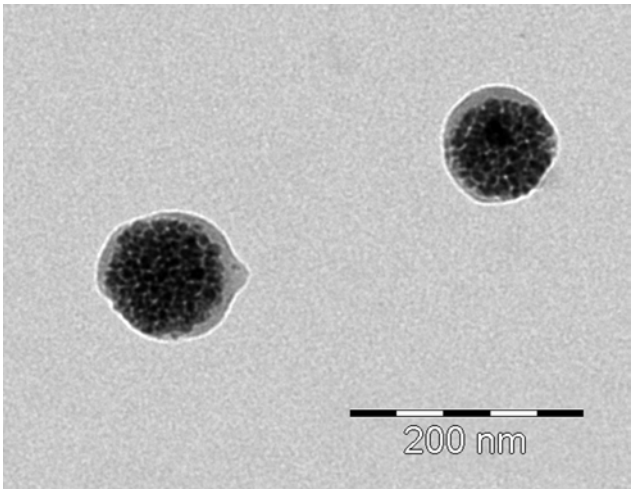

FIG. 1. Image of transmission electron microscopy of magnetic nanoparticles MagP-OH.

was made of 54 wt% methyl methacrylate, 15 wt% hydroxyl ethyl methacrylate and 31 wt% ethylene glycol dimethacrylate. As a consequence of this polymeric coating MagP-OH particles were functionalized with hydroxyl groups. We also used Phosphate Buffered Saline (PBS) with $MgCl_2$ and $CaCl_2$, liquid, sterile-filtered, suitable for cell culture, supplied by Sigma-Aldrich (Spain). In addition, we used a solution of $CaCl_2$ of 0.02 g/mL to initiate the cross-linking of the fibrinogen contained in the plasma. For this, we employed $CaCl_2$ powder (calcium chloride dehydrate, Sigma Ultra, Minimum 99.0%) provided by Sigma-Aldrich to prepare a $CaCl_2$ solution and Milli-Q water (Millipore). Finally, we used a solution of tranexamic acid (Amchafibrin 500 mg tablets, ROTTAPHARM, S.L.) in Milli-Q water at a concentration of 0.1 g/mL to prevent hydrogel fibrinolysis.

2.2 Preparation of the hydrogels and magnetic hydrogels

We prepared hydrogels following the protocol described by Alaminos and coworkers.[50] Briefly, for an initial volume of the mixture of 5 mL, we placed 3.8 mL of human plasma in culture dishes of 10 mL of volume and 35 mm of diameter. Then, we added 875 μL of PBS, 75 μL of tranexamic acid and 250 μL of 2% calcium chloride aqueous solution to promote the fibrin polymerization. Approximately 120 min after placing the hydrogels in the incubator, we added 5 mL of PBS (0.1 M and pH 7.2-7.4) to the obtained hydrogels to prevent their dehydration. Hydrogels were kept under cell culture conditions (37 ºC with 5% CO_2) for about 24 hours. Note that it is necessary to test these acellular hydrogels under these specific technical conditions, which are essential in most of the tissue engineering applications to ensure the cell function and viability.

We also prepared magnetic hydrogels by modifying slightly the previous protocol. Namely, adding the corresponding amount of MagP-OH nanoparticles dispersed into the PBS solution with a final volume of 875 μL. We tested different volume concentrations of MagP-OH particles in the initial mixtures, i.e. before the PBS addition after 2 hours, within the range 0.1 to 1 vol. %.

2.3 Macroscopic structure of hydrogels

We analyzed the macroscopic structural characteristics of the hydrogels by direct observation with an optical microscope (Nikon, SMZ800) at 5x of magnification. We took photos of hydrogels prepared by different experimental protocols by using a CCD camera (Pixelink, Canada) connected to the microscope.

2.4 Swelling of hydrogels

In order to have an indirect evaluation of cross-linking density and information about the hydrogel porous structure, we measured the mass of the pristine hydrogels after 24 hours of gelling. For this aim, we proceeded as it follows. (i) Hydrogels, contained in the culture dishes and submerged in PBS according to the preparation protocol (see subsection 2.2), were carefully detached from the walls of the dishes with the help of a spatula. (ii) We removed all the supernatant PBS solution contained in the dish with a pipette. (iii) Afterwards, we measured the mass of the dish containing the hydrogel ($M_{d\text{-}h}$) by means of a digital microbalance. (iv) We finally obtained the mass of the hydrogel, by subtracting the mass of the dish from $M_{d\text{-}h}$.

Furthermore, we obtained the mass of the hydrogels after dehydration. For this aim, we dried the hydrogels for 24 hours at 37 ºC in an oven in order to obtain the mass of their dry residue.

We executed this study only for those hydrogels that presented a macroscopically homogeneous structure and that were not broken by simple manipulation. For each concentration of magnetic particles, we performed these measurements a minimum of 3 times for different pristine hydrogels. Results shown in this work represent the average and standard deviation of each set of measurements. From these data, we obtained the volume-based swelling degrees Q of the hydrogels, which can be defined as:[51]

$$Q = \frac{V_p + V_{lc}}{V_p} \quad (1)$$

where V_p is the volume of polymer in the hydrogel and V_{lc} the volume of the liquid carrier medium. In our case, we proceeded as it follows. We approximated the mass of fibrin polymer to the mean mass of fibrinogen within human plasma: 2 g/L.[52] Then, we calculated the volume of polymer by taking into account the density of proteins, which is generally assumed equal to 1.35 g/mL independent of the nature of the protein and particularly independent of its molecular weight.[53] Thus, the estimated value of the volume of polymer in our hydrogels was V_p = 5.6 μL. Then, since as described above, we measured the volume of the hydrogels, we calculated Q by the following formula:

$$Q = \frac{V_T - V_{mp}}{V_p} \quad (2)$$

where V_T is the total volume of the hydrogels and V_{mp} is the volume of magnetic particles in the hydrogel, which is known from the preparation protocol. Note finally that we obtained V_T from the mass of the hydrogels by assuming a density of 1 g/mL, since water was their main constituent.

2.5 Microstructure of the hydrogels

For the analysis of the microscopic structure of the samples, we prepared samples by the technique of Critical Point Drying (CPD), which allows conservation of the original structure of the sample. Briefly, CPD technique consists of two steps: i) substitution of the water of the sample by carbon dioxide to avoid the alteration of the samples during the process; ii) elimination of the carbon dioxide by increasing temperature and pressure to reach critical point. After preparation following this protocol, we analyzed the internal microstructure of the hydrogels by means of a Quanta 650 Field-Emission Environmental Scanning Electron Microscope

(FEI, USA). In order to detect differences in composition, we used a circular back scatter detector, which allows determining differences in the composition of the observed matter within a single plane. With this technique, within a single observation plane denser elements appear brighter.

2.6 Rheological characterization of the hydrogels

We characterized the mechanical properties of the hydrogels with a Haake MARS III (Thermo Fisher Scientific, Waltham, MA, USA) controlled stress rheometer at 37 °C. Note that since the hydrogels were prepared in culture dishes they had a disk-like shape, with a diameter of 3.5 cm. Accordingly, we selected a measuring system geometry consisting of a parallel plate set of 3.5 cm of diameter with rough surfaces (to avoid wall slip) made of titanium (sensor P35Ti L, Thermo Fisher Scientific, Waltham, MA, USA). In order to perform the rheological measurements, we took the hydrogels out of the culture dishes and immediately after placed them on the bottom plate of the rheometer. Afterwards, we descended the upper plate of the rheometer until perfect contact with the hydrogel was reached, without appreciable compression of the hydrogel. We checked that this condition was satisfied when the normal force reached a value of 0.5 N. The corresponding gap thickness was approximately 200 µm in all cases (with a deviation smaller than 5%). Note that we used a fresh sample for each measurement and that measurements were performed in a water-saturated atmosphere to prevent from solvent loss. We investigated the rheological properties of the hydrogels under constant shear stress and also under oscillatory shear strains. For this aim we proceeded as it follows.

2.6.1 Behavior under constant shear stress. In these tests the samples were subjected to a constant shear stress and the corresponding shear strain was monitored as a function of time for 600 s (Fig. 2). As observed, for each value of the imposed shear stress, the strain increased fast with time during the first 50-100 s, tending to a stationary value at longer times. Thus, in this work we took the average of the strain corresponding to the last 100 s of curves like these shown in Fig. 2, as representative value of the shear strain for each imposed value of the shear stress. Measurements were repeated at increasing shear stress values. In this way, we obtained the curves of the stationary shear strain as a function of the imposed shear stress. The initial slope of these curves is the rigidity modulus of the hydrogels.

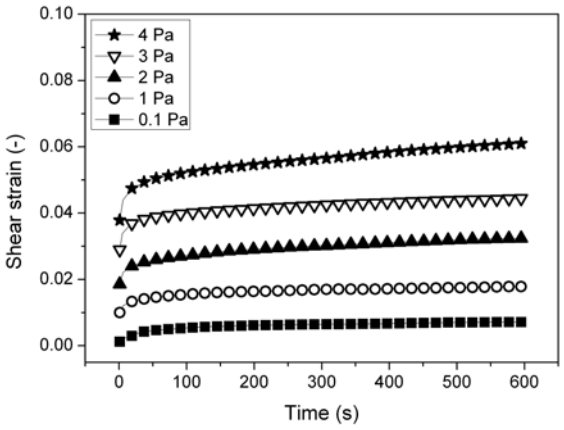

FIG. 2. Time evolution of the shear strain for different imposed values of the shear stress (indicated in the graph), for a nonmagnetic fibrin hydrogel.

2.6.2 Behavior under oscillatory shear strain. In these tests the samples were subjected to sinusoidal shear strains of given amplitude and frequency, and the corresponding shear stress was measured. We performed two types of tests for this regime: (i) Amplitude sweeps, for which the frequency of the oscillatory shear strain was fixed at 1 Hz and its amplitude increased logarithmically spaced in the range 0.005–2.0. This test allowed obtaining the linear viscoelastic region (LVR), for which the measured stress followed a sinusoid of the same frequency of the strain, although delayed by a lag angle. (ii) Frequency sweeps, for which we fixed the amplitude of the oscillatory shear stress at a value corresponding to the LVR, and the frequency was increased linearly spaced in the range of 0-10 Hz.

2.7 Investigation of gel formation by rheological measurements

Finally, we investigated the kinetics of gel formation by Winter Chambon criterion, using FTMS technique. For this aim, we used the Haake MARS III controlled stress rheometer, provided with a double cone-plate sensor of 60 mm of diameter and 2 º of apex angle and made of titanium (sensor DC60/2° Ti L, Thermo Fisher Scientific, Waltham, MA, USA). The temperature of the sample was fixed at 37 ºC. In these experiments, hydrogels were formed in the double cone-plate sensor following the same protocol described in paragraph 2.2, adjusting the total volume of the mixture to 8 mL. Then, for the total duration of the experiments, and starting immediately after the mixture was poured in the sensor of the rheometer, we subjected the cross-linking mixture to an oscillatory signal consisting of a combination of a sinusoidal waveform with several of its harmonics. Then, the dynamic viscoelastic parameters corresponding to each frequency were obtained by comparison of the Fourier Transform of the input and response waveforms, using the Software Haake RheoWin 4.60.0001 of Thermo Fisher Scientific. We took care of not exceeding the LVR, by fixing the total amplitude of the signal (summation of the signals corresponding to all harmonics) at a value of 0.7 Pa. At the same time, we checked that the resolution of measurement before the gel point was adequate. Finally, note that we worked at frequencies in the range 1 – 10 Hz.

2.8. *Ex vivo* biocompatibility analyses

In order to determine the *ex vivo* biocompatibility of nonmagnetic and magnetic hydrogels, we isolated human fibroblasts from healthy donors, expanded them until passage 5 and finally encapsulated them into the hydrogels at a cellular density of 1.3 x 10^5 cells/mL. For the encapsulation of cells into fibrin-based hydrogels and magnetic hydrogels we used well described protocols.[54-57] Hydrogels with cells were kept in

culture conditions (37ºC, 5% CO_2) with DMEM culture medium (supplemented with antibiotics and antimycotics cocktail solution and 10% fetal bovine serum (all from Sigma Aldrich, Germany). After 48h, we evaluated the *ex vivo* biocompatibility by using histology and DNA quantification as described previously.[56,58]

For histological and histochemical analyses, we fixed hydrogels for 24 h at room temperature with 3-4% neutral buffered formaldehyde. Once fixed, we dehydrated the samples, cleared and embedded them in paraffin and, finally we sectioned them at 5 µm. We dewaxed and stained the histological sections with hematoxylin-eosin and Perls' histochemical method for the specific identification of the MNP.[56]

In order to have quantitative values related to irreversible cell membrane damage, we quantified the released DNA by spectrophotometry as described previously. [56,58] Briefly, after the 48 h we removed the culture media, placed them in Eppendorf tubes and determined the concentration of DNA by using a NanoDrop 2000 UV-Vis Spectrophotometer (Thermo Fisher Scientific). We used four samples from each experimental condition, and recorded three determinations for each condition (n=12 each). In this study, we used constructs incubated with 2% Triton x-100 as negative control for each experimental condition. Additionally, as 2D positive technical controls of DNA spectrophotometry, we cultured cells into chamber slides (2D culture) and quantified DNA. Whereas, as 2D negative technical control we used cells cultured in chambers slides incubated with 2% Triton x-100. Furthermore, we determined the DNA presented in the culture medium and we subtracted these values from the results obtained from the hydrogels with cells and cells cultured in chamber slides.

2.8.1 Statistical analyses. In order to determine the impact on the biocompatibility of the incorporation of MNP into the fibrin hydrogels, we analyzed statistically the quantitative values of DNA. We subjected variables to Shapiro-Wilk test for normality and used Student's t-test for statistical comparisons. In this work we present all data as mean ± standard deviation. In addition, we determined statistical comparison with SPSS v16.00 software and considered $p<0.05$ values statistically significant in two-tailed tests.

2.8.2. Ethics statement. This study was approved by the Ethics Committee of the University of Granada, Granada, Spain. Each tissue donor for the culture of fibroblasts signed an informed consent form for the study.

3 Results

3.1 Macroscopic structure of hydrogels

At first sight, we could see that the hydrogels without MNP had a semi-transparent soft yellow color due to the human plasma employed (see Fig. 3a). On the other hand, magnetic hydrogels presented a brown color due to the MNP dispersed into the polymeric matrix (Fig. 3b). Nevertheless, in spite of the presence of MNP, magnetic hydrogels presented a homogeneous pattern from the macroscopic point of view (see Fig. 3c).

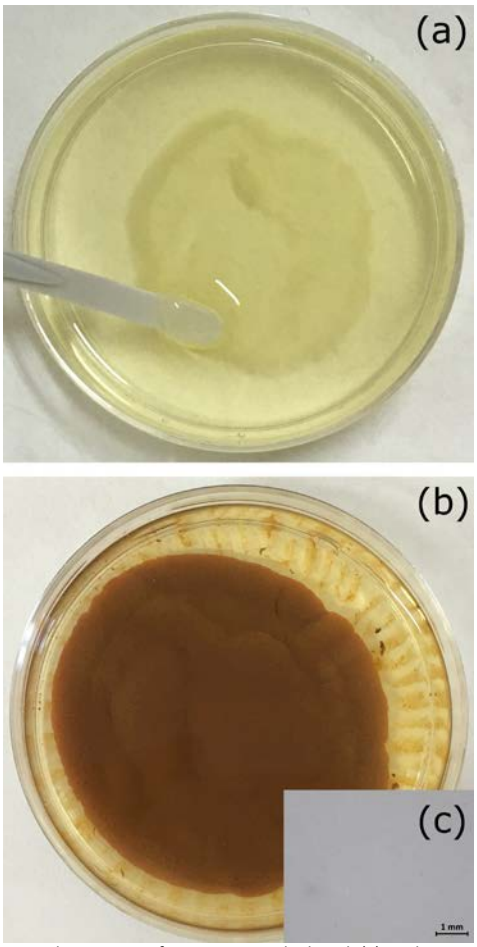

FIG. 3. Photography images of nonmagnetic hydrogel (a) and magnetic hydrogel prepared at a concentration of magnetic nanoparticles of 0.3 vol.% (b). (c) Optical microscopy image of magnetic hydrogel prepared at a concentration of magnetic nanoparticles of 0.2 vol.%.

In addition, we noticed that magnetic hydrogels corresponding to an initial concentration of MNP of 0.5% or higher presented a lumpy appearance and were rather fragile, so that it was difficult or impossible to manipulate them without breakage. On the contrary, hydrogels with initial concentration smaller than 0.5 % presented an appropriate consistency, being optimum for manipulation. Consequently, we focus in this work mainly on the hydrogels with a MNP concentration smaller than 0.5 %.

3.2 Swelling behavior of hydrogels

For fresh samples after 24 hours of preparation, magnetic hydrogels corresponding to concentrations of MNP of 0.1 % or 0.2 % presented a considerable higher weight than hydrogels without MNP (see Table 1). As the concentration of MNP was further increased above 0.2 %, the weight of the samples diminished, becoming non-significantly different with respect to nonmagnetic hydrogels. The maximum weight was thus obtained for a MNP concentration of 0.1 %, although no

Table 1. Experimental data corresponding to swelling experiments of hydrogels. We provide data of weight (W_i) and volume-based swelling degrees (Q) of hydrogels after 24 hours of incubation at 37 ºC, as well as weight (W_d) of hydrogels after dehydration. We can observe that the maximum Q value was obtained for fibrin hydrogels of 0.1 % concentration of magnetic particles.

Concentration of magnetic particles (% vol.)	W_i (mg)	Q (-)	W_d (mg)	W_d/W_i (%)
0	2630 ± 230	470 ±40	86 ± 25	3.3 ± 1.2
0.1	3800 ± 300	680 ± 50	112 ± 17	2.9 ± 0.7
0.2	3560 ± 200	640 ± 40	94 ± 22	2.6 ± 0.8
0.3	2540 ± 210	450 ± 40	117 ± 14	4.6 ± 0.9
0.4	2600 ± 400	460 ± 70	123 ± 15	4.7 ± 1.3

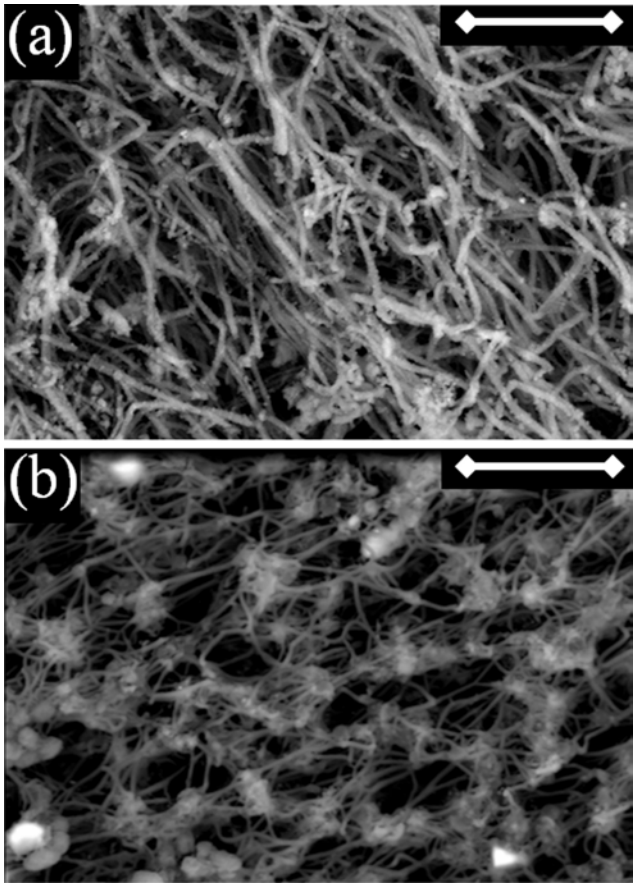

FIG 4. Environmental scanning electron microscopy of hydrogels. (a) nonmagnetic hydrogel; (b) magnetic hydrogel prepared at a concentration of magnetic nanoparticles of 0.2 vol.%.

significant difference was obtained for the weight of this sample with respect to the sample containing 0.2 %. Since the main contribution to the weight of the hydrogels was water (remark the almost negligible weight of the dried hydrogels with respect to their initial weight in Table 1), differences were mainly due to the water content, which was thus higher for magnetic hydrogels containing 0.1 % or 0.2 % of MNP, than for magnetic hydrogels containing a further concentration of MNP or nonmagnetic hydrogels. Furthermore, for dried samples differences in weight were minimal and statistically non-significant (note that average values are overlapped when standard deviations are taken into account), as a consequence of the removal of water.

The same conclusions can be drawn in terms of the volume-based swelling degrees (Q) –see data in Table 1. Nevertheless, this index gives us a better idea of the capacity of the polymer network to swell and, thus, of their maximum porosity achieved. Note the very high values of the swelling degree of both magnetic and nonmagnetic hydrogels. A Q value of 500 is more than 5 times higher than the maximum value reported by Messing and coworkers for poly(acrylamide) ferrohydrogels.[51] Concerning the non-monotonic dependence of the swelling degree on the concentration of MNP, it can be explained by supposing that the MNP may serve as nucleation sites for the fibrin polymerization. At the lowest concentration of MNP, their presence as knots of the fibrin net can open the network, resulting in a more porous structure. Then, as the concentration of MNP was increased, the additional cross-linking they imparted would progressively close the network, diminishing the porosity of the structure, and thus the swelling degree. Note that this hypothesis is consistent with the results of the next subsection.

3.3 Microstructure of the hydrogels

To verify this assumption of the particles opening the polymeric network, we carried out scanning electron microscopy (SEM) observations of nonmagnetic hydrogels and magnetic hydrogels containing 0.2 vol.% of MagP-OH nanoparticles. In such a way, we could observe that the nonmagnetic hydrogel (see Fig. 4a) had fibrin fibers distributed forming a relatively dense porous structure. Furthermore, we can see that the structure had not any junction, except for the homogeneously distributed links between couples of fibers. On the other hand, for magnetic hydrogels with 0.2 vol.% MagP-OH (see Fig. 4b), we observe a much opener structure, with knots formed presumably by clusters of MNP and polymer material (fibrinogen) –note that within a single plane of observation, denser elements appear brighter, which allows detecting the presence of magnetic particles. These knots very likely performed as cross-linkers between long polymer fibers, making possible to maintain an opener structure, avoiding the collapse of the fibers. Also, we can see that the structure was very homogeneous, with a high porosity that justifies the higher swelling capability of magnetic hydrogels compared with the swelling capability of the nonmagnetic hydrogels.

Let us finally mention that similar microstructures to these of Fig. 4b were observed for magnetic hydrogels with

concentration of magnetic particles smaller than 0.5 vol.% (pictures not shown here). On the other hand, for larger particle concentrations the amount of clusters within the samples largely dominated over connecting polymer fibers (pictures not shown here for brevity), which is consistent with failure of formation of macroscopically homogeneous hydrogels, in agreement with macroscopic observations of fragile hydrogels with lumpy appearance –see macroscopic observations in section 3.1.

3.4. Rheological characterization of the hydrogels

3.4.1 Behavior under constant shear stress. The behavior of the hydrogels was first characterized by measuring the shear strain resulting from imposed values of shear stress increased stepwise. At low shear strain the curves of shear stress vs. shear strain could be approximated to straight lines, with a characteristic slope (Fig. 5). This slope is the rigidity modulus, which is one of the quantities that are used to measure the stiffness of a material. For magnetic hydrogels, rigidity modulus increased with the concentration of MNP (Fig. 6). This increase is much stronger than this predicted by Einstein's formula or any other formula, such as Krieger-Dougherty equation, based on the assumption of hard, or slightly deformable spheres.[59] Note that such equations work well for random dispersion of the particles, without attachment to the polymers, as illustrated for example for magnetic hydrogels consisting of carrageenan and carbonyl iron particles in Ref. [60]. For the system under study, the enhancement of the rigidity modulus with the concentration of MNP is well fitted by a parabolic-like function, as this of the model presented in section 4.1 below.

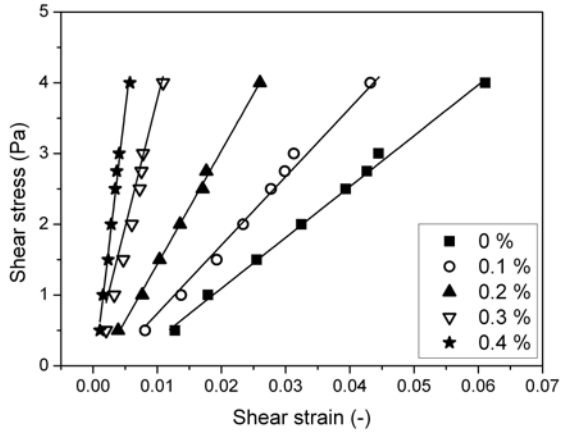

FIG. 5. Shear stress vs. shear strain curves for fibrin hydrogels prepared at different volume concentrations of magnetic nanoparticles (indicated in the figure). Symbols represent experimental data and the continuous lines the best fits to straight lines. Experimental data were obtained from curves like those shown in Fig. 2, by average of the shear strain values corresponding to the last 100 s of measurement.

3.4.2 Behavior under oscillatory shear strain. For the characterization of the behavior under oscillatory shear strain, first we carried out oscillatory shear tests of fixed frequency (1 Hz) and increasing strain amplitude. From these measurements we obtained the values of *G*' and *G*'' as a function of the strain amplitude (γ). An example of the obtained curves of *G*' and *G*'' vs. γ is shown in Fig. 7 –note that similar trends were obtained for other magnetic hydrogels, as well as for nonmagnetic hydrogels. Let us analyze the trends obtained for curves of *G*' and *G*'' vs. γ. First, as observed, the curves demonstrate roughly constant values of *G*' and *G*'' at low values of the strain amplitude (γ <0.03). This pseudoplateau region is identified with the LVR. At larger values of the strain amplitude, both *G*' and *G*'' progressively diminished, in what is known as the nonlinear viscoelastic regime. Within the complete LVR, the values of *G*' are much larger than the values of *G*'', which is an indication of the material being more solid-like than liquid-like, in coherence with what is expected for a cross-linked material. On the other

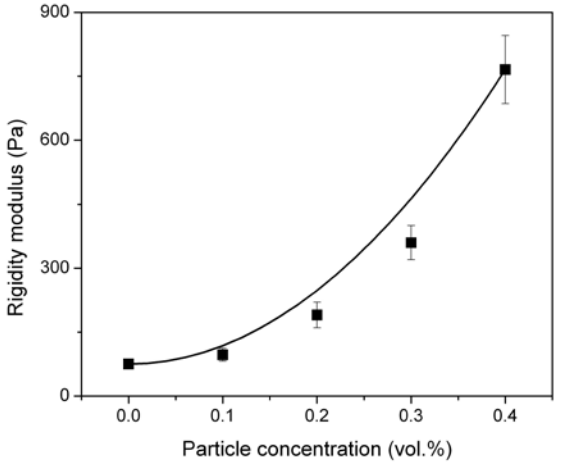

FIG. 6. Rigidity modulus of magnetic hydrogels for increasing concentration of magnetic nanoparticles. Squares represent the experimental data. The continuous line (-) represents the theoretical prediction according to equation (12), for $G_0 = 75\ Pa; A = 4.3 \cdot 10^7\ Pa$.

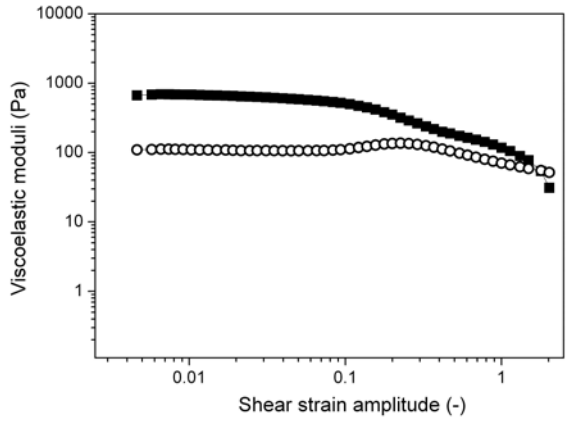

FIG. 7. Storage (■) and loss (○) moduli as a function of shear strain amplitude for oscillatory measurements at a frequency of 1 Hz for a magnetic hydrogel prepared at a concentration of magnetic nanoparticles of 0.2 vol.%.

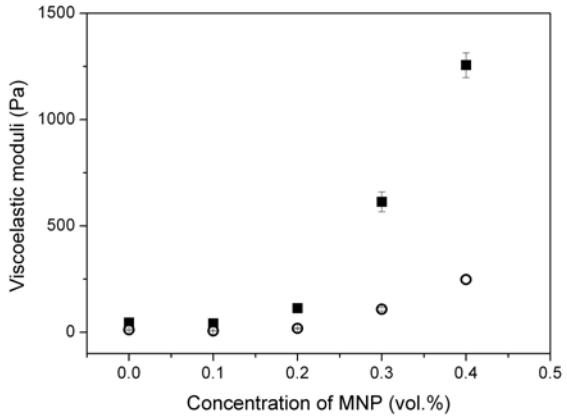

FIG. 8. Storage modulus (■) and loss modulus (○) corresponding to the viscoelastic linear region, as functions of the concentration of magnetic nanoparticles (MNP), for fibrin hydrogels.

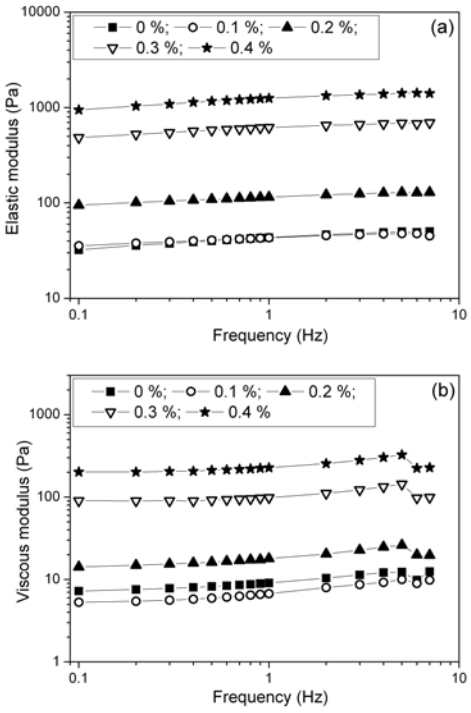

FIG. 9. Storage modulus (a) and loss modulus (b) as a function of frequency for fibrin hydrogels prepared at different concentrations of magnetic nanoparticles (indicated in the graphs).

hand, at very large values of the strain amplitude within the nonlinear viscoelastic regime, there is a crossover of G' and G'' at a given threshold value of γ, above which the viscous dissipation of energy (proportional to G'') dominates over the elastic storage of energy (proportional to G').

In order to compare the viscoelastic moduli of the different hydrogels (magnetic and nonmagnetic) it is appropriate to take the value of the viscoelastic moduli within the LVR as the representative value for each hydrogel. As observed, both quantities increased strongly with the content of MNP, similarly to the case of the rigidity modulus (Fig. 8). In fact, the storage modulus was approximately 20 times higher for the magnetic hydrogel with the highest content of nanoparticles (0.4 vol.%) than for the nonmagnetic hydrogels –a similar relative increase was obtained for the loss modulus.

Table 2. Experimental data corresponding to the critical shear strain value that marks the onset of the nonlinear viscoelastic regime.

Concentration of magnetic particles (% vol.)	Critical shear strain (-)
0	0.060 ± 0.011
0.1	0.087 ± 0.009
0.2	0.067 ± 0.007
0.3	0.045 ± 0.005
0.4	0.0216 ± 0.0022

Another important rheological parameter that can be obtained from curves like these shown in Fig. 7 is the critical strain that delimits the limit of the LVR. Several authors have identified this critical strain as the point where the storage modulus deviates 10% from the plateau value.[61,62] We used the same criterion in this work and obtained that the value of the critical strain increased for concentration of MNP of 0.1 vol.% with respect to the nonmagnetic hydrogel (Table 2). Then, as the concentration of MNP was further increased above 0.1 vol.%, a tendency of the critical strain to decrease with MNP concentration was obtained (Table 2). Remark that the overall trend correlates with this obtained for Q values (see Table 1). Note at this point that for colloidal gels, a similar non-monotonic dependence was recently found for the trend of the storage modulus as a function of the preshear strain.[63] In this previous work, this non-monotonic dependence showed an inverse correlation with the volume of the empty space in the gel. In the case of the present work, we may consider that the increase of the critical strain for 0.1 vol.% is connected to changes in the microstructure of this magnetic hydrogel (where particle knots took the roll of cross-linkers), with respect to nonmagnetic hydrogel (where only intersections between pairs of polymer fibers were observed). Then, as the concentration of MNP was increased, the polymer network became less porous, as demonstrated by swelling experiments, and at the same time more rigid with respect to deformation, as inferred from the decrement of the critical strain. In addition, this hypothesis of particle knots as cross-linkers would also justify the monotonic dependence of the storage modulus with the MNP content, as discussed in section 4.

In addition to oscillatory tests of fixed frequency and increasing amplitude, that are useful for the determination of the extension of the LVR, we performed oscillatory tests of fixed strain amplitude (within the LVR) and increasing frequency. From these measurements we obtained the viscoelastic moduli as a function of the frequency. The typical trend for G' consisted of a very slight tendency to increase with frequency (Fig. 9a). The overall trend for G'' consisted of a

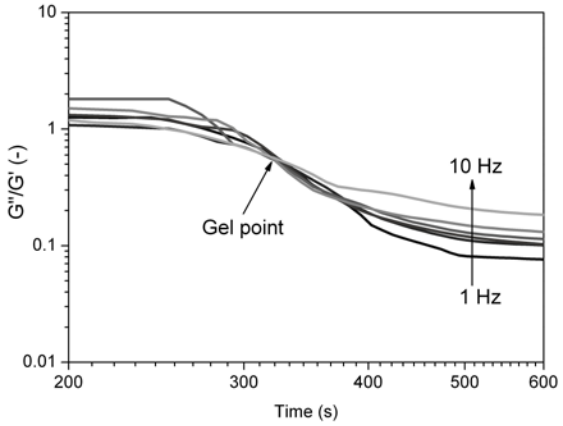

FIG. 10. tan **δ=** *G''*/ *G'* measured simultaneously at different frequencies by Fourier Transform Mechanical Spectroscopy for a nonmagnetic fibrin hydrogel (similar results were obtained for magnetic hydrogels).

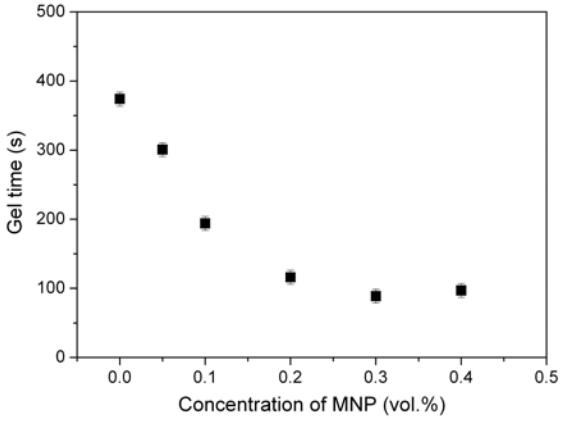

FIG. 11. Time for gel point according to Winter Chambon criterion, as a function of the concentration of magnetic nanoparticles (MNP) for fibrin hydrogels.

stronger (with respect to *G'*) tendency to increase up to a frequency of 5 Hz, followed by a decrease at higher frequencies (Fig. 9b). In addition, in all cases *G'* was larger than *G''* for the whole range of frequencies (compare Fig. 9a and Fig. 9b). Again, these tendencies obtained for our hydrogels are typical of cross-linked polymer systems.[64]

3.5 Investigation of gel formation by rheological measurements

Finally, we investigated the kinetics of gelling by Winter Chambon criterion using FTMS technique. From these experiments we obtained the viscoelastic moduli within the LVR as a function of time for several frequencies. Then, we plotted the curves of tanδ=G''/G' vs. time and identified the gel time as the point at which tanδ was frequency independent (see Fig. 10 as an example). Results demonstrated that time required for gel point decreased with particle content (Fig. 11). It is also remarkable the fact that the mere presence of 0.1 vol.% of magnetic particles gave rise to a decrease of time for gel point by a factor of 2 with respect to the hydrogel without magnetic particles. We can explain these results by assuming that MNP created additional points of cross-linking with respect to nonmagnetic hydrogels and, as a consequence, the cross-linking process took place faster, the higher the concentration of MNP up to a concentration of 0.4 vol.%.

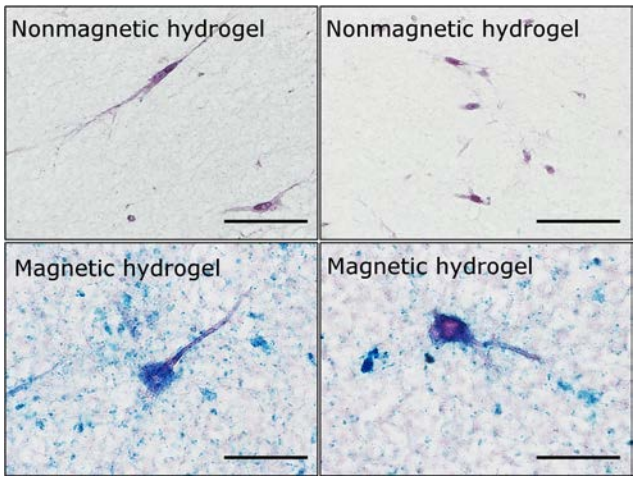

FIG. 12. Ex vivo histological and histochemical analyses of fibroblast cultured in nonmagnetic fibrin hydrogels and magnetic fibrin hydrogels. H-E staining (corresponding with the two pictures above) confirm the presence of several fibroblasts with their characteristics cytoplasmic processes cultured in nonmagnetic fibrin hydrogels, whereas Perls's histochemical method (corresponding with the two pictures below) shows the distribution of the magnetic nanoparticles in magnetic fibrin hydrogels. Note that several magnetic nanoparticles interact with the fibroblast surface. Scale bar= 50 μm.

Table 3. Quantitative and statistical results for DNA-released biocompatibility assay.

	Nonmagnetic hydrogel	Magnetic hydrogel	2D cell culture
DNA-release	218 ± 5[a]	284 ± 14[a,b,c]	25 ± 9[a,b]
DNA-release Negative control	592 ± 5	676 ± 4	2013 ± 18

Note: Values for DNA-released analysis are shown as the mean ± standard deviation. Units for DNA mean values are ng/µl. Values for the negative controls for each condition (DNA-release Negative controls) correspond to the DNA-release after the incubation with Triton X-100. Comparison between different groups was carried out using the Student's t-test.

[a] Statistically significant differences between positive values vs. negative controls.

[b] Statistically significant differences vs. nonmagnetic hydrogel.

[c] Statistically significant differences between magnetic hydrogels vs. 2D cell culture technical control.

3.6 Ex vivo biocompatibility

Histological analyses revealed that the fibroblasts were successfully encapsulated into both the nonmagnetic and the magnetic fibrin hydrogels. After 48 h under culture conditions, these cells showed their typical elongate shape and some filopodia were identified in both nonmagnetic and magnetic hydrogels, suggesting an adequate cell-biomaterial interaction (Fig. 12). The Perls' histochemical method was positive for the MNP showing that they were homogeneously distributed into

the fibrin hydrogel. Interestingly, an intense Perls' positive reaction was observed around the fibroblast surface suggesting a possible interaction of these MNP with these cells (Fig. 12).

The quantification of DNA-released revealed that cells under 3D culture condition showed significantly higher values ($p<0.05$) as compared to the cells cultured under 2D conditions (Table 3). However, each experimental condition showed significantly lower values in comparison to the negative controls ($p<0.05$), which confirm the biocompatibility of both the nonmagnetic and the magnetic hydrogels. Nevertheless, when we compared the DNA-release values between the nonmagnetic hydrogels and the magnetic hydrogels we found a statistically significant ($p<0.05$), slight increase for the latter.

4 Discussion and theory

We characterized experimentally the physical properties of fibrin-based magnetic hydrogels for different concentrations of magnetic particles (from 0 up to 0.4 vol.%), consisting of a magnetite core and a layer of polymers with OH^- functionalization. Analysis of the microstructure demonstrated that in the absence of MNP the hydrogel presented a porous network of fibrin fibers with an isotropic distribution of the polymers (Fig. 4a). The addition of MNP resulted also in an isotropic network of fibrin fibers that, however, was disrupted by the presence of large clusters (Fig. 4b). These clusters consisting of nanoparticles and fibrin polymers constituted the knots of attachment of the network's filaments. Attraction between the positive groups of the fibrinogen, from which fibrin was polymerized, and the negative OH^- groups of the magnetic particle surface may justify the formation of these clusters. In fact, fibrin fibers were formed by polymerization of fibrinogen (from blood plasma) in the presence of Ca^{2+} ions. Fibrinogen is a glycoprotein consisting of three different chains (α, β, and γ), linked to each other by disulfide bonds and forming a central E domain (negatively charged), two identical peripheral D domains (negatively charged), and two αC domains (positively charged).[65-67] The conversion of fibrinogen to fibrin takes place in several steps: (i) thrombin cleaves fibrinopeptides A and B located on the N-terminus of the fibrinogen α and β chains respectively of the E domain. As a result, soluble fibrinogen turns into a monomer of fibrin, with a positively charged E domain.[68] (ii) Fibrin monomers interact via electrostatic interactions (of the positively charged E domains with the D domains of negative charge) followed by hydrogen bonding to form a non-covalently linked fibrin polymer. (iii) Crosslinking of this polymer to form a covalently linked fibrin polymer (clot) is catalyzed by the transglutaminase enzyme (Factor XIIIa), which forms amide bonds between the ε-amino group of a lysine residue and the γ-carboxamide group of a glutamine residue of adjacent D domains.[69] MagP-OH nanoparticles had negative surface charge as a consequence of the OH^- functionalization. Then, according to the previous explanation of the formation of fibrin from fibrinogen, fibrinogen molecules very likely adsorbed on MagP-OH MNP prior to thrombin cleavage (step (i)) because of the electrostatic attraction between the negative OH^- groups of MagP-OH MNP and the positively charged αC domains of fibrinogen molecules. Note that a similar explanation for the adsorption of fibrinogen on negatively charged inorganic materials was previously reported in the literature.[70] As a consequence, fibrinogen molecules were expected to anchor on the MagP-OH MNP and acted as condensation sites for the subsequent polymerization of fibrin fibers, in agreement with observations in Fig. 4b. Furthermore, this positive interaction between fibrinogen and MNP would justify the faster cross-linking process of magnetic hydrogels with respect to nonmagnetic hydrogels. In fact, it is reasonable to conclude that the higher the concentration of cross-linker, the faster the time for reaching the gel point. In this regard, note that Growney Kalaf and co-workers found that the gel time of alginate hydrogel decreased as the concentration of cross-linker (calcium ions) was increased, in agreement with our hypothesis.[71]

The rheological analysis demonstrated a progressive enhancement of the rigidity modulus (Figs. 5 and 6) and the viscoelastic moduli (Figs. 7-9) as the content of MNP was increased. For the largest concentration of MNP (0.4 vol.%) we obtained rigidity and viscoelastic moduli more than one order of magnitude larger than for nonmagnetic hydrogels. This enhancement seems consistent with the observed changes in the microstructure and we could conclude that the presence of MNP reinforced the polymer structures. In fact, the classical theory of gel elasticity demonstrates that the storage modulus of a gel is proportional to the concentration of polymer subchains that link the junctions of the gel network.[72] As we can see for example in the Fig. 4b clusters cross-link the fibrin threads. An important feature observed in this figure is that two clusters can be bounded by several fibrin threads. This would justify the observed growth of the hydrogel mechanical properties with the concentration of the MNP. In subsection 4.1 below, we provide a theoretical model based on the previous experimental observations, which allows explaining the observed trend of the rigidity modulus on the concentration of magnetic particles.

Concerning the viscoelastic behavior of our hydrogels, we found that in all cases (magnetic and nonmagnetic hydrogels) the storage modulus dominates over the loss modulus (Figs. 7-9), as expected for cross-linked polymer systems.[64] In general terms, the trends obtained for the viscoelastic moduli as a function of the frequency of the oscillatory shear strains within the LVR (Fig. 9) are also typical of cross-linked polymer systems. The tendency of the storage modulus (G') to increase very smoothly with frequency was previously observed for artificial tissues of human oral mucosa stroma prepared from fibrin-based hydrogels,[73] as well as in the case of native tissue of human vocal fold mucosa[74] that consists mainly of a network of type I and III collagen and elastin fibers. Regarding the tendency of the loss modulus (G'') to increase with frequency, with some rather strong decrease at frequencies larger than approx. 5 Hz in most of the cases, something similar was obtained previously for artificial tissues of human oral mucosa stroma prepared from fibrin-based hydrogels.[73]

Furthermore, Chan and Titze reported a similar trend for the damping factor of native human vocal fold mucosa.[74]

4.1 Theoretical model for the rigidity modulus

The main goal of this subsection is to explain the principal physical cause of the non-linear dependence of the rigidity modulus of the magnetic hydrogels on the volume concentration of the MNP. In agreement with experimental observations and the previous discussion, we suppose that due to interaction of the MagP-OH nanoparticles with the fibrinogen, the particles and the fibrinogens condense into dense clusters, alike to these of Fig. 4b. These clusters play the role of attachment knots in the systems of the fibrin threads. Let us denote the number of the thread segments (sub-chains) in the unit volume of the composite as ν. The classical theory of gel net elasticity gives –see, for example Ref.[19,72]

$$G \sim kT\nu \qquad (3)$$

This formula can be applied to gels, where the sub-chains present Gaussian (ideal) macromolecular coils, as it is presumably the case for nonmagnetic hydrogels. The only characteristic energy of these coils is the thermal energy kT. However, this is not the case for the magnetic hydrogel under consideration. The macromolecular segments observed by SEM (e.g., Fig. 4b) seem to be flexible linear threads, but not bulk coils. Taking this into account we can generalize Eq. (3) as:

$$G \sim w\nu \qquad (4)$$

Here w is some typical energy of change of the sub-chain conformation. The microscopic determination of this energy requires detailed analysis of these transformations of the fibrin chain, which is a complex problem, beyond the scope of the present work. Here we will estimate w by fitting Eq. (4) to the experimental results.

It is natural to suppose that the mean number of the sub-chains, linking with a single cluster, is proportional to the drop (cluster) surface. Consequently, we can write:

$$\nu \sim n_d S_d \xi \qquad (5)$$

Here n_d is the numerical concentration (number per unit volume) of the clusters, S_d is the drop surface, ξ is number of contacts of the fibrin threads with the cluster per unit of the drop surface. This parameter is determined by the details of interaction between the fibrinogens as well as of the fibrinogens with the particles. Since these details are unknown, we will consider ξ as an empirical parameter. Further, the following relation of conservation of the total number of particles can be used:

$$n_d V_d \varphi_d \sim \varphi_0 \qquad (6)$$

Here φ_0 and φ_d are total volume concentration of the particles in the composite and their concentration inside the drops respectively, and V_d is the drop volume. By combination of Eqs. (5) and (6) we get:

$$\nu \sim \xi \frac{\varphi_0}{\varphi_d} \frac{S_d}{V_d} \sim \xi \frac{\varphi_0}{\varphi_d} V_d^{-1/3} \qquad (7)$$

Where the relation $S_d \sim V_d^{2/3}$ has been taken into account. Note, of course, that the experimental clusters were not identical, presenting some slight variation in their size and state of surface. Because of this, S_d and ξ must be considered as some typical, mean magnitudes. After mixture of the MagP-OH nanoparticles with the polymer, this mixture (suspension) of particles and fibrinogens is supersaturated. Then, the condensation of the particles, adsorbed on the fibrinogens, into the dense drops takes place. As well-known from the general theory of the condensation phase transition, volume of the viable nuclei of new phase must be more than some critical volume V_c. For the spherical-like nuclei, the critical volume, roughly, can be estimated as:[75]

$$V_c^{-1/3} \sim \frac{1}{\sigma} p_0 \qquad (8)$$

Here σ is the surface tension of the drop, and p_0 is the osmotic pressure in the main part of the solution. Taking into account that the volume concentrations of both the particles and the fibrinogens in the hydrogel are low, we can use the following estimate of the osmotic pressure of dilute two-component solution:

$$p_0 = kT\left(\frac{\varphi_0}{v_p} + \frac{\varphi_f}{v_f}\right) \qquad (9)$$

Here v_p and v_f are respectively the volumes of the particles and fibrinogen, and φ_f is the volume concentration of the fibrinogens at the moment of the nucleation. We can suppose that initially the supersaturation of the particle-fibrinogen system was high and, consequently, this system experienced a sudden (instantaneous) nucleation. Due to the fast rate of the nucleation, the supersaturation decreased quickly, and the rate of drop growth diminished very fast. Furthermore, polymerization of fibrins out of the drops should also contribute to the interruption of the drops evolution. Thus, in a first approximation, we can suppose the instantaneous stop of the growth of the drops right after their appearance. This means that volume of the viable drops is approximately equal to the critical volume V_c. Note, that clusters observed experimentally were similar, presenting only a slight variation in their size (see Fig. 4b as an example). This supports the hypothesis on the instant nucleation of the system.

By combination of Eqs. (4), (8) and (9), by using V_c instead of V_d in (7), we come to the following estimate:

$$G \sim kT\left(\frac{w}{\sigma}\right)\xi\frac{\varphi_0}{\varphi_d}\left(\frac{\varphi_0}{v_p}+\frac{\varphi_f}{v_f}\right)+G_0 \quad (10)$$

Here G_0 is the shear modulus of the pure gel, without the MNP, which accounts for the fact that even in the absence of MNP, the fibrin fibers are cross-linked into a gel. From the experimental observations we estimated the volume and volume concentration of the fibrinogens as: $v_f \sim 10^8 nm^3$, $\varphi_f \sim 0.1–0.2\%$. The average volume of a single MagP-OH magnetic nanoparticle is $v_p \sim 10^6 nm^3$. Thus, for the studied hydrogels with the particle volume concentration $\varphi_0 \geq 0.1$ % the following strong inequality is fulfilled:

$$\frac{\varphi_0}{v_p} >> \frac{\varphi_f}{v_f} \quad (11)$$

Under this consideration, Eq. (10) can be written as:

$$G \sim A\varphi_0^2 + G_0 \quad (12)$$

with $A = kT\left(\frac{w}{\sigma}\right)\frac{\xi}{\varphi_d v_p}$.

We can estimate parameter A by using the experimental results. For example, for $\varphi_0 = 0.4\%$ we get $A \approx 4 \cdot 10^7$ Pa. From the experimental observations we can also estimate other parameters. In particular, we obtained $w \sim 10^{-16}$ J and $\xi \sim 10^{13}$ m^{-2}, which are reasonable values from the physical point of view. Comparison of the experimental results with the theoretical ones is shown in Fig. 6. The agreement with the experimental results and the formula given by Eq. (12) is quite reasonable. Thus, at least from the semiquantitative point of view, our model explains the experimental trend, which can be taken as a justification of our hypotheses.

Conclusions

The incorporation of MNP functionalized with polymers bearing OH^- groups in a fresh mixture of human plasma and calcium chloride results in magnetic hydrogels after some induction time at 37 ºC. For a nanoparticle concentration smaller than 0.5 vol.% in the initial mixture, the resulting hydrogels are macroscopically homogeneous, with the nanoparticles embedded in the fibrin polymer network. These magnetic hydrogels are highly porous and have high swelling behavior. We have found that the porosity largely increases for the hydrogels with a concentration of 0.1 vol.% of MNP with respect to the nonmagnetic hydrogels. Then, as the concentration of MNP is further increased above 0.1 vol.%, a progressive decrease of porosity takes place. Microscopic observations suggest that nanoparticles create some clusters that serve as knots for the cross-linking of the fibrin fibers. Interestingly, magnetic hydrogels also show superior mechanical properties (larger rigidity and viscoelastic moduli) as compared with nonmagnetic hydrogels. In fact, for a concentration of MNP of 0.4 vol.% in the initial mixture, the mechanical moduli of the resulting magnetic hydrogel are more than 1 order of magnitude higher than these of the nonmagnetic hydrogels. Furthermore, we have also shown that the time for gel point obtained according to Winter Chambon criterion diminishes as the concentration of MNP increases. The reason for this enhancement of the mechanical properties of magnetic hydrogels seems to be connected to the role of nanoparticles as cross-linkers of the polymer network, as a result of the attraction between the negative OH^- groups of the particle surface and the positive groups of the plasma fibrinogen. In fact, we have developed a theoretical model based on this hypothesis that semiquantitatively predicts the experimental values of the rigidity modulus. The theoretical explanation of the strong dependence of the rigidity modulus of the hydrogel on the concentration of the nanoparticles is based on the indirect attraction of fibrinogen monomers through the attachment to particles. Due to this attraction fibrinogen condenses into nuclei of a dense phase. Evolution of these aggregates slows down with time due to the decrease of the fibrinogen supersaturation and the decrease of their mobility because of the gel polymerization. By the end of the polymerization, the nuclei (knots) of the dense phase cross link the fibrin threads, which justifies the enhancement of the mechanical properties. Furthermore, we have demonstrated the *ex* vivo biocompatibility of magnetic hydrogels and, thus, we can conclude that the presence of the MNP does not alter cell viability. As a consequence of their high porosity and stronger mechanical properties, hydrogels with properly functionalized embedded particles should be preferred for biomedical applications, such as scaffolds for tissue engineering. To conclude, we have elucidated the physical reasons and requirements for the preparation of such a kind of nanocomposite hydrogels with superior structural and mechanical properties. We envisage that the results of our work will be of help for the generation of other similar systems as well as for conceiving new applications.

Acknowledgements

This study was supported by project FIS2013-41821-R (Plan Nacional de Investigación Científica, Desarrollo e Innovación Tecnológica, Ministerio de Economía y Competitividad, Spain, co-funded by ERDF, European Union) and by grant FIS PI14-1343 (Spanish Plan Nacional de Investigación Científica, Desarrollo e Innovación Tecnológica, from the National Ministry of Economy and Competitiveness -Instituto de Salud Carlos III; co-financed by Fondo Europeo de Desarrollo Regional –FEDER-, European Union). J.M.A. acknowledges financial support by CNPq through its postdoctoral fellowship program (Ref. No. 203100/2014-0). A.Z is also grateful to the Russian Fund for Basic Research, 16-58-12003, the Program of Russian Federation Ministry of Science and Education, project 3.1438.2017/PCh. Dr. Laura Rodríguez-Arco is acknowledged

for helpful discussion. This work is part of the PhD thesis of A.B.B.-E.

Notes and references

1 G. D. Nicodemus and S. J. Bryant, *Tissue Engineering Part B: Reviews*, 2008, **14** (2), 149.
2 S. Ladet, L. David and A. Domard, *Nature*, 2008, **452**, 76-79.
3 A. Atala, S. B. Bauer, S. Soker, J. J. Yoo and A. B. Retik, *Lancet*, 2006, **367**, 1241.
4 N. Boucard, C. Viton, D. Agay, E. Mari, T. Roger, Y. Chancerelle and A. Domard, *Biomaterials*, 2007, **28**, 3478.
5 I. A. Rodriguez, M. T. López-López, A. C. Oliveira, M. C. Sánchez-Quevedo, A. Campos, M. Alaminos and J. D. G. Durán, *Journal of Tissue Engineering and Regenerative Medicine*, 2012, **6** (8), 636.
6 V. Carriel, J. Garrido-Gomez, P. Hernandez-Cortes, I. Garzon, S. Garcia-Garcia, J. A. Sáez-Moreno, M. C. Sánchez-Quevedo, A. Campos and M. Alaminos, *Journal of Neural Engineering*, 2013, **10**, 026022.
7 L. García-Martínez, F. Campos, C. Godoy-Guzmán, M. C. Sánchez-Quevedo, I. Garzon, M. Alaminos, A. Campos, and V. Carriel, *Histochemistry and Cell Biology*, 2016, doi: 10.1007/s00418-016-1485-9.
8 Langer, R. New methods of drug delivery, *Science*, 1990, **249**, 1527.
9 S. Mitragotri and J. Lahann, *Nature Materials*, 2009, **8**, 15-21.
10 N. W. Choi, M. Cabodi, B. Held, L. Gleghorn, J. Bonassar, A. D. Stroock, *Nature Materials*, 2007, **6**, 908.
11 S. Aktas, D. M. Kalyon, B. M. Marin-Santibanez,J. Perez-Gonzalez, *Journal of Rheology*, 2014, **58**, 513.
12 P. C. Nalam, N. N Gosvami, M. A. Caporizzo b, R. J. Composto, R. W. Carpick, *Soft matter*, 2015, **11**, 8165.
13 V. Adibnia, R. J. Hill, Journal of Rheology, 2016, **60**, 541.
14 D. Bonn, M. M. Denn, Science, 2009, **324**, 1401.
15 J. M. Piau, *Journal of Non-Newtonian Fluid Mechanics*, 2007, **144**, 1.
16 D. Calvet, J. Y. Wong, S. Giasson, *Macromolecules*, 2004, **37**, 7762.
17 J. Cho, M. C. Heuzey, M. L. Hamdine, *Macromolecular Materials and Engineering*, 2007, **292**, 571.
18 D.J. Curtis, A. Holder, N. Badiei, J. Claypole, M. Walters, B. Thomas, M. Barrow, D. Deganello, M.R. Brown, P.R. Williams, K. Hawkins, *Journal of Non-Newtonian Fluid Mechanics*, 2015, **222**, 253.
19 M. Rubistein and R. H. Colby, Polymer Physics, Oxford University, New York, NY, 2003.
20 H. H. Winter, F. Chambon, Journal of Rheology, 1986, **30**, 367.
21 H. H. Winter, *Polymer Engineering and Science*, 1987, **27**, 1698.
22 F. Chambon, H. H. Winter, *Journal of Rheology*, 1987, **31**, 683.
23 E. E. Holly, S. K. Venkataraman, F. Chambon, H. H. Winter, *Journal of Non-Newtonian Fluid Mechanics*, 1988, **27**, 17.
24 K. Hawkins, M. Lawrence, P. R. Williams, R. L. Williams, *Journal of Non-Newtonian Fluid Mechanics*, 2008, **148**, 127.
25 E. Ghiringhelli, D. Roux, D. Bleses, H. Gilliard, F. Caton, Rheologica Acta, 2012, **51**, 413.
26 Y. Li, G. Huang, X. Zhang, B. Li, Y. Chen, T. Lu, T. J. Lu and F. Xu, *Advanced Functional Materials*, 2013, **23** (6), 660.
27 M. T. Lopez-Lopez, G. Scionti, A. C. Oliveira, J. D. G. Duran, A. Campos, M. Alaminos and I. A. Rodriguez, *Plos One*, 2015, **10** (7): e0133878. doi:10.1371/journal.pone.0133878.
28 J. I. Kim, B. Kim, C. Chun, S. H. Lee and S.-C. Song, Biomaterials, 2012, **33**, 4836.
29 L. Rodriguez-Arco, I. A. Rodriguez, V. Carriel, A. B. Bonhome-Espinosa, F. Campos, P. Kuzhir, J. D. G. Duran and M. T. Lopez-Lopez, *Nanoscale*, 2016, **8**, 8138.
30 M. T. Lopez-Lopez, I. A. Rodriguez, L. Rodriguez-Arco, V. Carriel, A. B. Bonhome-Espinosa, F. Campos, A. Zubarev and J. D. G. Duran, *Journal of Magnetism and Magnetic Materials*, 2016. doi: 10.1016/j.jmmm.2016.08.053
31 M. Bañobre-López, Y. Piñeiro-Redondo, R. De Santis, A. Gloria, L. Ambrosio, A. Tampieri, V. Dediu and J. Rivas, *Journal of Applied Physics*, 2011, **109**, 07B313.
32 N. Bock, A. Riminucci, C. Dionigi, A. Russo, A. Tampieri, E. Landi, V. A. Goranov, M. Marcacci and V. Dediu, *Biomaterialia*, 2010, **6**, 786.
33 B. Das, M. Mandal, A. Upadhyay, P. Chattopadhyay and N. Karak, *Biomedical Materials*, 2013, **8**: 035003.
34 R. De Santis, A. Gloria, T. Russo, U. D'Amora, S. Zeppetelli, C. Dionigi, A. Sytcheva, T. Herrmannsdo, V. Dediu and L. Ambrosio, *Journal of Applied Polymer Science,* 2011, **122**, 3599.
35 A. Gloria, T. Russo, U. D'Amora, S. Zeppetelli, T. D'Alessandro, M. Sandri, M. Bañobre-López, Y. Piñeiro-Redondo, M. Uhlarz, A. Tampieri, J. Rivas, T. Herrmannsdörfer, V. A. Dediu, L. Ambrosio and R. De Santis, *Journal of the Royal Society Interface*, 2013, **10**, 20120833.
36 S. H. Hu, T. Y. Liu, C. H. Tsai and S. Y. Chen, Journal of Magnetism and Magnetic Materials, 2007, **310**, 2871.
37 H. Hu, W. Jiang, F. Lan, X. Zeng, S. Ma, Y. Wu and Z. Gu, *RSC Advances*, 2013, **3**, 879.
38 K. Lai, W. Jiang, J. Z. Tang, Y. Wu, B. He, G. Wang and Z. Gu, *RSC Advances*, 2012, **2**, 13007.
39 S. Panseri, C. Cunha, T. D'Alessandro, M. Sandri, G. Giavaresi, M. Marcacci, C. T. Hung and A. Tampieri, *Journal of Nanobiotechnology*, 2012, **10**, 32.
40 H. Skaat, O. Ziv-Polat, A. Shahar, D. Last, Y. Mardor and S. Margel, *Advanced Healthcare Materials*, 2012, **1**, 168.
41 A. Tampieri, E. Landi, F. Valentini, M. Sandri, T. D'Alessandro, V. Dediu and M. A. Marcacci, *Journal of Nanotechnology*, 2011, **22**, 015104.
42 A. Tampieri, T. D'Alessandro, M. Sandri, S. Sprio, E. Landi, L. Bertinetti, S. Panseri, G. Pepponi, J. Goettlicher, M. Bañobre-Lopez and J. Rivas, *Acta Biomaterialia*, 2012, **8**, 843.
43 X. B. Zeng, H. Hu, L. Q. Xie, F. Lan, Y. Wu and Z. W. Gu, *Journal of Inorganic Materials*, 2013, **28**, 79.
44 Y. Zhu, F. Shang, B. Li, Y. Dong, Y. Liu, M. R. Lohe, N. Hanagata and S. Kaskel, *Journal of Materials Chemistry B*, 2013, **1**, 1279.
45 O. Ziv-Polat, H. Skaat, A. Shahar and S. Margel, *International Journal of Nanomedicine*, 2012, **7**, 1259.
46 R. K. Singh, K. D. Patel, J. H. Lee, E. J. Lee, J. H. Kim, T. H. Kim and H. W. Him, *Plos One*, 2014, **9**, e91584.
47 X. B. Zeng, H. Hu, L. Q. Xie, F. Lan, W. Jiang, Y. Wu and Z. W. Gu, *International Journal of Nanomedicine*, 2012, **7**, 3365.
48 H. M. Yun, S. J. Ahn, K. R. Park, M. J. Kim, J. J. Kim, G. Z. Jinc, H. W. Kim and E. C. Kim, *Biomaterials*, 2016, **85**, 88.
49 R. M. Christensen, Mechanics of Composite Materials. Malabar: Krieger Publishing Company; 1991.

50 M. Alaminos, M. Del Carmen Sanchez-Quevedo, J. I. Munoz-Avila, D. Serrano, S. Medialdea, I. Carreras and A. Campos, *Investigative Ophthalmology and Visual Science*, 2006, **47**, 3311.

51 R. Messing, N. Frickel, L. Belkoura, R. Strey, H. Rahn, S. Odenbach and A. M. Schmidt, *Macromolecules*, 2011, **44**, 2990.

52 T. Lang, K. Johanning, H. Metzler, S. Piepenbrock, C. Solomon, N. Rahe-Mayer, K. A. Tanaka, Anesthesia & Analgesia, 2009, **108** (3), 751.

53 H. Fischer, I. Polikarpov and A. F. Craievich, *Protein Science,* 2004, **3**, 2825.

54 V. Carriel, G. Scionti, F. Campos, O. Roda, B. Castro, M. Cornelissen, I. Garzón, M. Alaminos, *Journal of Tissue Engineering and Regenerative Medicine*, 2015, doi:10.1002/term.2039

55 L. García-Martínez, F. Campos, C. Godoy-Guzmán, M. C. Sánchez-Quevedo, I. Garzón, M. Alaminos, A. Campos, V. Carriel, *Histochemistry and Cell Biology*, 2017, **147,** 83-95.

56 V. Carriel, I. Garzón, A. Campos, M. Cornelissen, M. Alaminos, *Journal of Tissue Engineering and Regenerative Medicine*, 2017, **11**, 553.

57 F. Campos, A. B. Bonhome-Espinosa, L. García-Martínez, J. D. G. Duran, M. T. López-López, M. Alaminos, M. C. Sánchez-Quevedo, V. Carriel, *Biomedical Materials*, 2016, **11,** 055004. doi:10.1088/1748-6041/11/5/055004.

58 M. A. Martin-Piedra, I. Garzon, A. C. Oliveira, C. A. Alfonso-Rodriguez, V. Carriel, G. Scionti, M. Alaminos, *Cytotherapy*, 2014, **16**, 266.

59 R. G. Larson, The Structure and Rheology of Complex Fluids. Oxford University Press, 1999.

60 T. Mitsumata, A. Honda, H. Kanazawa, M. Kawai, *The Journal of Physical Chemistry B*, 2012, **116**, 12341.

61 I. Agirre-Olabide, M. J. Elejabarrieta, M. M. Bou-Ali, *Journal of Intelligent Material Systems and Structures*, 2015, **26**, 1880.

62 N. M. Wereley, A. Chaudhuri, J. H. Yoo, *Journal of Intelligent Material Systems and Structures*, 2006, **17**, 393.

63 E. Moghimi, A. R. Jacob, N. Koumakis, G. Petekidis, *Soft Matter*, 2017, doi: 10.1039/c6sm02508k.

64 C. W. Macosko, Rheology: principles, measurements and applications. Wiley-VCH, Weinheim, 1994.

65 A.V. Bychkova, O.N. Sorokina, A.L. Kovarski, A.B. Shapiro, V.B. Leonova and M.A. Rozenfel'd, *Biophysics*, 2010, **55**, 544.

66 H.C.F. Cote, S.T. Lord, K.P. Pratt, *Blood*, 1998, **92**, 2195.

67 P. Zeliszewska, A. Bratek-Skicki, Z. Adamczyk, M. Ciesla, *Langmuir*, 2014, **30**, 11165.

68 G. Hudry-Clergeon, G. Marguerie, L. Pouit, M. Suscillon, *Thrombosis Research*, 1975, **6**, 533.

69 M. W. Mosesson, Journal of Thrombosis and Haemostasis, 2005, **3**, 1894.

70 N. Hassan, V. Verdinelli, J.M. Ruso and P.V. Messina, Soft Matter, 2012, **8**, 6582.

71 E. A. Growney Kalaf, R. Flores, J. Gary Bledsoe, S. A. Sell, *Materials Science and Engineering*, 2016, **63**, 198.

72 A. Grosberg, A. Khokhlov, A. Statistical Physics of Macromolecules, Springer, Berlin, 1994.

73 M. A. Rodriguez, M. T. López-López, J. D. G. Durán, M. Alaminos, A. Campos and I. A. Rodriguez, *Cryobiology*, 2013, **67**, 355.

74 R. W. Chan, I. R. Titze, *Journal of Acoustical Society of America*, 1999, **106**, 2008.

75 L.P. Pitaevskii, E.M. Lifshits, Physical Kinetics, Butterworth-Heinemann, 1999, 452p.